THE JOURNAL OF PHYSICAL CHEMISTRY B

Article

pubs.acs.org/JPCB

Excited-State Dynamics of an Environment-Sensitive Push–Pull Diketopyrrolopyrrole: Major Differences between the Bulk Solution Phase and the Dodecane/Water Interface

Sabine Richert,[†] Sandra Mosquera Vazquez,[†] Marek Grzybowski,[‡] Daniel T. Gryko,[‡] Alexander Kyrychenko,[§] and Eric Vauthey*[,†]

[†]Department of Physical Chemistry, University of Geneva, 30 quai Ernest-Ansermet, CH-1211 Geneva 4, Switzerland

[‡]Institute of Organic Chemistry of the Polish Academy of Sciences, 01-224 Warsaw, Poland

[§]V. N. Karazin Kharkiv National University, 4 Svobody Square, Kharkiv 61022, Ukraine

Supporting Information

ABSTRACT: The excited-state dynamics of a diketopyrrolopyrrole (DPP) derivative with push–pull substituents has been investigated in a variety of solvents and at the dodecane/water and dodecane/heavy-water interfaces using a combination of ultrafast spectroscopic techniques, including transient electronic absorption and time-resolved surface second-harmonic generation. Whereas the photophysics of a nonpolar DPP analogue is mostly independent of the solvent, the fluorescence decay of the push–pull DPP accelerates strongly by going from aprotic to protic solvents. As this effect increases with the polarity and the hydrogen-bond-donating ability of the solvent, it is attributed to the occurrence of H-bond-assisted nonradiative deactivation induced by the charge-transfer character of the excited state that favors the coupling of the molecule to the H-bond network of the solvent. At the dodecane/water interface, the excited-state lifetime is longer by a factor of ca. 20 than that estimated in pure water and increases further by a factor of about 3 when going to the dodecane/heavy-water interface. This isotope effect, that is more than twice as strong as that measured in bulk solutions, and molecular dynamic simulations indicate that the slowing down of the dynamics at the interface cannot be solely ascribed to a reduced accessibility of the DPP molecule to the aqueous phase. The slower excited-state decay is rather assigned to the conjunction of several effects, such as the strengthening of the H-bond network formed by the interfacial water molecules and the lower local polarity of the interfacial region.

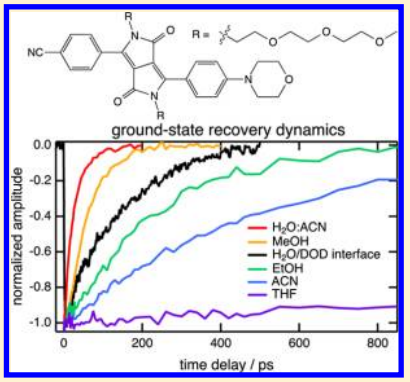

INTRODUCTION

Over the past few decades, substantial effort has been invested in understanding the properties of water at hydrophobic surfaces, as such interfaces play a crucial role in many areas of science and technology.[1−13] In organic synthesis, key chemical reactions, such as Diels–Alder cycloadditions and Claisen rearrangements, involving water-insoluble compounds have been found to be faster when in contact with water.[14−18] Although the origin of this accelerated reactivity is still not understood, it seems to be associated with some specific interaction between the reacting molecules and interfacial water.[19−22]

Vibrational surface sum frequency generation (SSFG) has been widely used to obtain structural information on interfacial water.[23−28] On the other hand, second-order nonlinear techniques based on an electronic resonance enhancement, such as electronic surface second-harmonic generation (SSHG) and electronic SSFG, although yielding less structural insight, are particularly powerful for investigating dye molecules adsorbed at an interface.[29−34] Electronic resonance enhancement allows the response from the adsorbed dyes to be easily discriminated from that of the solvent, although the latter is present at a much higher concentration. Additionally, these techniques can be relatively easily time-resolved, allowing the excited-state dynamics of molecules adsorbed at an interface to be investigated and compared to their solution-phase dynamics.[35,36] Such a comparison has proven to be very powerful in accessing the properties of liquid interfaces as a specific medium for chemical reactions.[37,38] This approach requires molecular probes with environment-dependent excited-state dynamics, such as triphenylmethane dyes, whose excited-state lifetime increases with the viscosity of the environment, making them useful friction probes for interfacial studies.[39−41]

We report here on an investigation toward a better understanding of the changes in chemical reactivity when going from solution phases to liquid/liquid interfaces. Toward this aim, we have studied the excited-state dynamics of a new diketopyrrolopyrrole (DPP) derivative (DPP1, Chart 1) in solution and at liquid interfaces using ultrafast transient

Received: June 18, 2014
Revised: July 28, 2014
Published: August 2, 2014

Chart 1. Structure of the Diketopyrrolopyrrole (DPP) Dyes

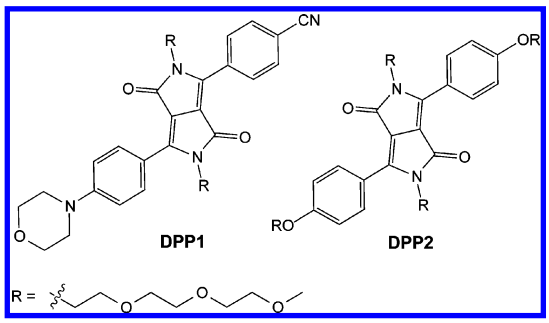

absorption and time-resolved SSHG (TR-SSHG), respectively. DPP dyes were originally known as red and orange pigments for paints, inks, and plastics.[42] More recently, their charge-carrier properties have also been recognized; therefore, these dyes are being increasingly applied for optoelectronic applications.[43−47] DPP1 was specially designed for interfacial studies, having two oligoethylene glycol chains to favor water solubility and push−pull groups, i.e., dialkylamino and nitrile substituents, to introduce charge-transfer character into the electronic excited state and to suppress the centrosymmetry of the chromophore.

Our original intention was to use this molecule as a polarity probe. However, as will be shown below, the introduction of charge-transfer character into the $S_1 \leftarrow S_0$ transition leads to dramatic changes in the photophysics of the molecule. Whereas the excited-state lifetime of DPP2, the centrosymmetric analogue of DPP1 (Chart 1), amounts to several nanoseconds independent of the environment, that of DPP1 decreases strongly with the polarity and the hydrogen-bond-donating properties of the solvent. Our TR-SSHG experiments, complemented by molecular dynamic (MD) simulations, reveal that this solvent dependence makes DPP1 a valuable probe for investigating H-bond interactions with interfacial water. We will show that the excited-state dynamics of this molecule changes considerably when going from solution phases to the dodecane/water interface.

This article is organized as follows: after the Experimental Section, the synthesis of DPP1 and DPP2 is first briefly presented; the excited-state properties of both dyes in bulk solutions are then described and their differences are discussed; finally the excited-state dynamics of DPP1 at the water/dodecane interface is presented, discussed with the help of the MD simulations, and compared to bulk-phase dynamics.

EXPERIMENTAL SECTION

Samples. Solvents cyclohexane (CHX), dodecane, dibutylether, chloroform, *n*-propylacetate, tetrahydrofuran, acetone, acetonitrile (ACN), methanol (MeOH), ethanol (EtOH), 1-propanol (PrOH), 1-butanol (BuOH), 1-pentanol (PeOH), 1-hexanol (HxOH), 1-decanol (DeOH), and D_2O were at least 99% pure and were used as received from either Acros Organics or Fischer Chemicals.

Spectroscopic Measurements. Absorption spectra were recorded on a Cary 50 spectrometer, whereas fluorescence emission and excitation spectra were recorded on a Cary Eclipse fluorimeter. All emission spectra were corrected for the wavelength-dependent sensitivity of the detector. The fluorescence quantum yields, Φ_f, were determined using fluorescein in 0.1 M NaOH as a reference (Φ_f = 0.93).[48]

Nanosecond fluorescence dynamics was measured by time-correlated single-photon counting (TCSPC), as described in refs 49 and 50 using 60 ps excitation pulses at 469 nm generated at 10 MHz by a laser diode (Picoquant, LDH-PC-470). The full width at half-maximum (fwhm) of the instrument response function (IRF) was around 200 ps.

Faster fluorescence dynamics were monitored by fluorescence upconversion (FU) as described elsewhere.[51,52] Excitation was performed at 400 nm with the frequency-doubled output of a Kerr-lens mode-locked Ti/sapphire laser (Mai Tai, Spectra Physics). The pump intensity on the sample was of the order of 5 $\mu J/cm^2$, and the fwhm of the IRF was ca. 200 fs. The sample solutions were located in a 0.4 mm rotating cell and had an absorbance of about 0.2 at 400 nm. Global analysis of the FU time profiles was performed as described in detail in ref 53.

The electronic transient absorption (TA) measurements have been carried out with the setup described in refs 54 and 55. Excitation was performed at 400 nm using the frequency-doubled output of a standard 1 kHz amplified Ti/sapphire system (Spectra Physics). The pump intensity on the sample was ca. 0.5 mJ/cm^2. The polarization of the probe pulses was at the magic angle relative to that of the pump pulses. The fwhm of the IRF was around 150 fs. The sample solutions were located in a 1 mm quartz cell and were continuously stirred by N_2 bubbling. Their absorbance at the excitation wavelength was around 0.2.

The time-resolved surface second harmonic generation (TR-SSHG) setup has been described in detail previously.[37,56] The pump pulses (∼80 fs, 1 μJ at the interface) were generated with a noncollinear optical parametric amplifier (TOPAS White, Light Conversion), whereas the probe pulses (∼100 fs, 0.2−0.5 μJ at the interface), were produced with a collinear optical parametric amplifier (TOPAS C, Light Conversion). Both optical parametric amplifiers were pumped by 1 mJ and 100 fs pulses at 800 nm generated by a 1 kHz Ti/sapphire amplified system (Solstice, Spectra-Physics). The pump pulses were circularly polarized and focused on the interface from the top using a combination of spherical and cylindrical lenses, whereas the probe pulses were focused with a 500 mm lens onto the interface at an angle of incidence of about 70° where they underwent total internal reflection. The SSHG signal was collected with a 100 mm lens, separated from the fundamental probe light with a short-pass filter and focused onto the entrance slit of a Czerny-Turner spectrograph (Shamrock 163, Andor) equipped with a multipixel cooled CCD camera (Newton 920, Andor). The illuminated pixels were vertically binned and summed over the wavelength range of interest, and the resulting value was transferred to a computer.

TR-SSHG measurements were performed at the dodecane/water and dodecane/D_2O interfaces. The samples were located in a 4 × 4 × 4 cm^3 quartz cell. As DPP1 was not sufficiently water-soluble, a stock solution of the dye in $CHCl_3$ was prepared. A certain amount of 1 nmol was deposited on 10 mL of water with the help of a syringe, and the solvent was evaporated. The upper phase, 12 mL dodecane, was added after about 10 min.

The nonresonant contribution to the SSHG signal measured without DPP1 was found to be negligibly small, i.e., within the noise of the signal. As a consequence, the SSHG signal measured with DPP1 has purely electronic resonance character, and its intensity is proportional to the square modulus of the relevant tensor element of the second-order nonlinear susceptibility tensor, $\vec{\chi}^{(2)}$. Unless specified, the probe pulses

dx.doi.org/10.1021/jp506062j | J. Phys. Chem. B 2014, 118, 9952−9963

Scheme 1. Synthesis of DPP1 and DPP2

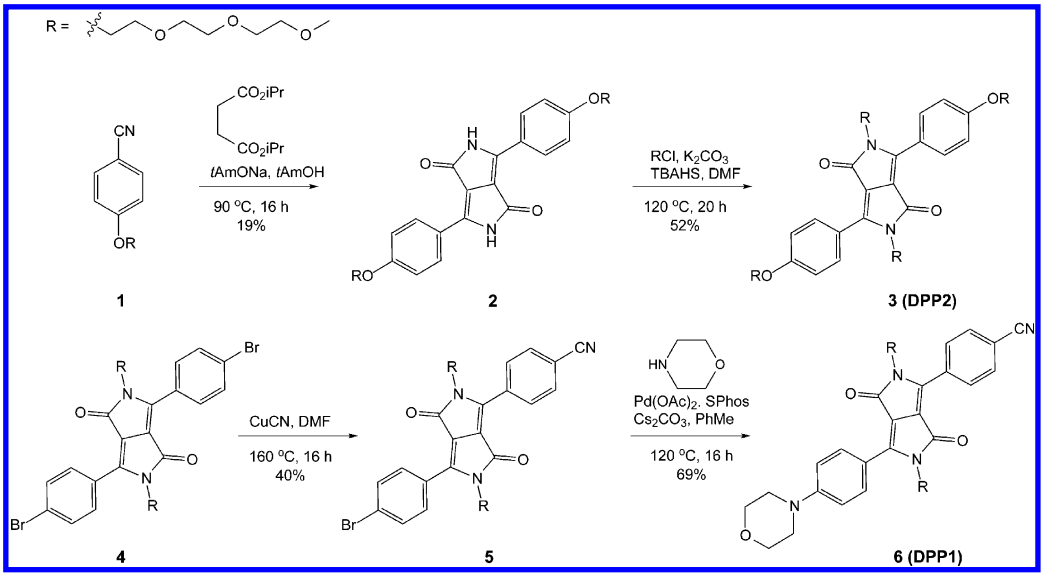

were s-polarized, i.e., along the x axis, and the p-polarized component of the SSHG signal was detected. In this case, the signal intensity is proportional to $|\chi^{(2)}_{zxx}|^2$, where the z axis is normal to the interface plane.

The TR-SSHG profiles were processed by first taking the square root of the measured SSHG intensity and then normalizing it so that the signal is zero at negative pump−probe delays and is equal to −1 at the strongest photoinduced signal depletion.[57] The resulting signal intensity, $S(t)$, is then proportional to the photoinduced population changes.

The stationary SSHG spectra were recorded using the same setup. The probe wavelength was scanned from 790 to 1070 nm using 10 nm steps. At each step, the SSHG intensity was detected within a spectral window of the CCD camera corresponding to half the probe wavelength. The probe pulse energy at the sample position was kept constant at 1 μJ. The reliability of the resulting spectra was confirmed by comparing the SSHG spectrum of malachite green with the electronic SSFG spectrum reported in ref 41.

Quantum Chemistry Calculations and Molecular Dynamics (MD) Simulations. Ground-state gas-phase geometry optimization was performed using density functional theory (DFT) with the M06 and the B3LYP functionals[58,59] and the 6-31G* basis set. Both functionals gave qualitatively the same results. The static second-order hyperpolarizability was calculated at the B3LYP/6-31G* level of theory. The electronic transitions were computed with time-dependent DFT (TD-DFT) using the B3LYP functional and the 6-31G* basis set. The calculations were carried out using Gaussian 09.[60]

MD simulations were performed with two different systems: DPP1 at the dodecane/water interface and in bulk water. The OPLS-AA force-field parameters for dodecane were adopted from ref 61 whereas the simple point charge (SPC) model was used for water.[62] The bond length and angle parameters of DPP1 were optimized using DFT calculations at the B3LYP/cc-pVDZ level, and the partial charges needed for the Coulomb interactions were derived from the B3LYP/cc-pVDZ electron densities by fitting the electrostatic potential to point (ESP) charges. The configuration interaction singles (CIS) method was used for the excited-state geometry and electric charges. The dodecane/water system was composed of 243 dodecane and 3193 water molecules. The initial systems were equilibrated for 10 ns, and the MD simulations were carried out for 100 ns at a constant number of particles, pressure P = 1 atm, temperature T = 303.15 K (NPT ensemble), and an integration time step of 2 fs. Three-dimensional periodic boundary conditions were applied with the z axis lying along a direction normal to the interface. The pressure was controlled semi-isotropically so that the x−y and z dimensions of the simulation box were allowed to fluctuate independently of each other, keeping the total pressure constant. The reference temperature and pressure were kept constant using the Berendsen weak coupling scheme with a coupling constant of τ_T = 0.1 ps for the temperature coupling and $\tau_{P(x-y)} = \tau_{P(z)}$ = 1.0 ps for the pressure coupling.[63] Electrostatic interactions were simulated with the particle mesh Ewald (PME) approach using the long-range cutoff of 0.8 nm.[64] The cutoff distance of Lennard-Jones interactions was also equal to 0.8 nm. All bond lengths were kept constant using the LINCS routine.[65] The MD simulations were carried out using the GROMACS set of programs, version 4.5.5.[66]

RESULTS AND DISCUSSION

Synthesis. The synthetic strategy for the preparation of DPP1 and DPP2 is shown in Scheme 1 and is described in detail in the Supporting Information. In brief, nitrile **1**, which was synthesized by the alkylation of *p*-hydroxybenzonitrile with triethylene glycol monomethyl ether tosylate, was submitted to the base-promoted condensation reaction with diisopropyl succinate under the standard conditions of DPP synthesis.[67] Desired product **2** was obtained in rather low yield (19%). The alkylation of that compound with triethylene glycol monomethyl ether chloride was performed at 120 °C in DMF using potassium carbonate as the base in the presence of a catalytic amount of tetrabutylammonium bisulfate (TBAHS) to give DPP2 in 52% yield. DPP2, possessing four triethylene glycol chains, appears as a fluorescent, amorphous orange solid. All attempts to recrystallize this compound failed, mainly because of its great solubility in nonpolar (toluene, hexane) as well as polar solvents (dimethylformamide, acetone, and methanol).

Push−pull molecule DPP1 was synthesized in two steps from dibrominated dye **3**, whose preparation is described in the

dx.doi.org/10.1021/jp506062j | J. Phys. Chem. B 2014, 118, 9952−9963

literature.[47] In the first step, the cyanide group was introduced by a reaction with copper(I) cyanide in DMF at 160 °C (Rosenmund−von Braun reaction), which gave monocyano derivative **4** in 40% yield. Together with desired dye **4**, a dicyanated byproduct (26%) and starting material **3** (23%) were also separated from the reaction mixture. Compound **4** was then transformed into final product DPP1 by the Buchwald−Hartwig reaction with morpholine, using Pd-$(OAc)_2$/SPhos as a catalyst and cesium carbonate as a base.

Steady-State Spectroscopy. The electronic absorption and emission spectra of DPP1 and DPP2 in ACN are shown in Figure 1. Their absorption spectra are dominated by a broad

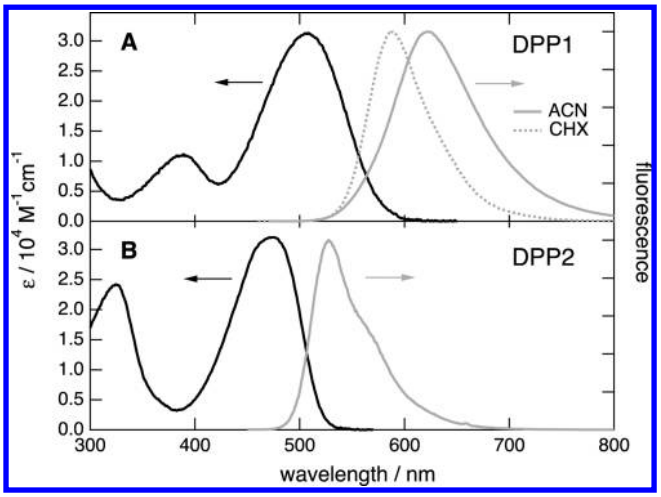

Figure 1. Electronic absorption and fluorescence spectra measured with (A) DPP1 and (B) DPP2 in acetonitrile. The fluorescence spectrum of DPP1 in cyclohexane is also shown for comparison.

and intense band culminating at 506 and 473 nm for DPP1 and DPP2, respectively. TD-DFT gas-phase calculations performed on analogues of the DPPs with the oligoethylene glycol chains on the N atoms replaced by methyl groups and those on the phenyl rings of DPP2 replaced by H atoms predict the first absorption band to be at 514 and 466 nm, respectively, and to originate from a one-electron transition from the highest occupied (HOMO) to the lowest unoccupied molecular orbital (LUMO).

Whereas for DPP2 both frontier orbitals are symmetric and delocalized over the whole chromophore, a marked redistribution of the electronic density from the phenylmorpholinyl side to the cyanophenyl unit can be observed for DPP1 (Figure 2) when going from the HOMO to the LUMO. This points to an S_1 state with substantial charge-transfer character, as intended when designing this molecule. Despite this, only a very modest solvatochromism of the absorption band of DPP1 can be observed (Figure S1): if only aprotic solvents are considered, the band position does not correlate with the solvent polarity but rather with its refractive index, with the band shifting from 508 nm in ACN (n = 1.346) to 516 nm in $CHCl_3$ (n = 1.446).

On the other hand, if only the protic solvents are considered, then an additional correlation with the hydrogen-bond donor strength of the solvent, quantified by Kamlet−Taft parameter α,[68] seems to be present, with a blue shift of the band from to 519 to 498 nm upon going from hexanol (α = 0.8, n = 1.418)[69] to water (α = 1.17, n = 1.33).[69] This solvent dependence indicates, first, that the ground state of DPP1 is weakly polar

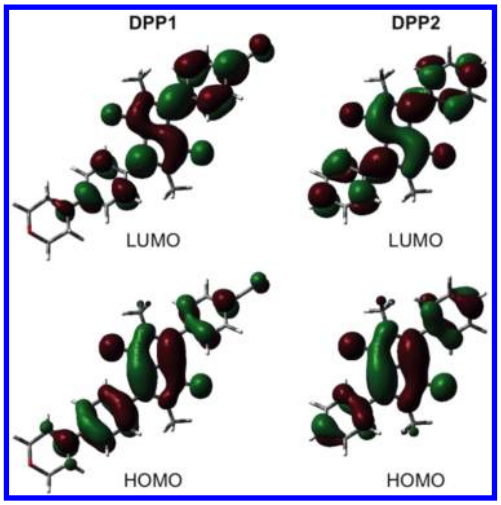

Figure 2. Frontier molecular orbitals of DPP1 and DPP2 computed at the B3LYP/6-31G* level of theory. The oligoethylene glycol chains on the N atoms have been replaced by methyl groups, and those on the phenyls (DPP2), by H atoms.

and its solvation energy is dominated by dispersion interactions in aprotic solvents and, second, that in protic solvents, H-bond interactions are also operative and apparently stabilize the ground state relative to the Franck−Condon excited state. The carbonyl oxygen atoms most probably play a key role in this latter interaction. Figure 2 reveals that the electronic density on one of these oxygen atoms decreases markedly, whereas that on the other oxygen atom increases slightly when going from the HOMO to the LUMO, pointing to different H-bonding strengths in the excited state.

Compared to DPP2, the fluorescence spectrum of DPP1 is broader and less structured, and in contrast to DPP2, DPP1 exhibits substantial solvatochromism (Figures 1 and S2A). In nonprotic solvents, the band shifts to lower energy with increasing solvent polarity, and a plot of the emission maximum in wavenumber vs the polarity function, $f(\varepsilon_s) = (\varepsilon_s - 1)/(\varepsilon_s + 2)$, where ε_s is the static dielectric constant, is linear with a slope of -1410 ± 70 cm^{-1} (Figure S2B). According to the Onsager model, this slope, expressed in joules, corresponds to $-\vec{\mu}_e\Delta\vec{\mu}/(4\pi\varepsilon_0 a^3)$, where $\vec{\mu}_e$ is the electric dipole moment in the excited state, $\Delta\vec{\mu}$ is the dipole moment difference between the excited and ground states, and a is the cavity radius.[70,71] If we assume, based on the weak solvatochromism of the absorption band, that the ground-state dipole moment of DPP1 is zero, then the slope reduces to $-\vec{\mu}_e^{\,2}/(4\pi\varepsilon_0 a^3)$. The latter expression, with a cavity radius of 4.74 Å deduced from the volume obtained from quantum chemical calculations, results in an excited-state dipole moment of $\vec{\mu}_e$ = 6 D. This value is only approximate but clearly confirms the charge-transfer character of the S_1 state of DPP1. In aprotic solvents, the fluorescence quantum yield, Φ_f, also varies with the solvent polarity, decreasing from 0.57 to 0.046 by going from CHX to ACN (Table 1).

By contrast, the fluorescence of DPP1 exhibits almost no solvatochromism in protic solvents, at least when going from MeOH to DeOH (Table 1). In the shorter alcohols, namely, PeOH to MeOH, the emission maximum is blue-shifted compared to that of aprotic solvents with similar $f(\varepsilon_s)$ values, with this shift increasing from PeOH to MeOH. As will be shown below, this effect can be ascribed to the excited-state lifetime of DPP1 that is much shorter in protic than aprotic

dx.doi.org/10.1021/jp506062j | J. Phys. Chem. B 2014, 118, 9952−9963

Table 1. Solvent Dependence of the Excited-State Properties of DPP1[a]

solvent	ε_s	α	λ_f/nm	Φ_f	τ_f/ps	τ_{TA}/ps
acetonitrile	37.5	0.19	622	0.046	460	465
acetone	21.4	0.08	618	0.16	2.0×10^3	
tetrahydrofuran	7.6	0	609	0.38	4.5×10^3	
propylacetate	6.0	0	604	0.42	4.4×10^3	
chloroform	4.8	0.20	601	0.44	4.6×10^3	
dibutylether	3.1	0	592	0.44	4.5×10^3	
cyclohexane	2.0	0	589	0.57	4.1×10^3	
H_2O	81.2	1.17		$<3 \times 10^{-4}$	<10	
H_2O/acetonitrile					15 (3:1)[b]	22, ~90 (1:1)[b]
H_2O/methanol					13 (1:1)[b]	
D_2O	79.8			$<5 \times 10^{-4}$		
D_2O/acetonitrile						26, 80 (1:1)[b]
methanol	33.5	0.98	614	3.9×10^{-3}	46	45
methanol-D_1					52	56
ethanol	25.3	0.86	614	0.017	220	220
1-propanol	20.8	0.84	613	0.037	470	
1-butanol	17.9	0.84	615	0.055	730	
1-pentanol	14.6	0.84	613	0.082	1.0×10^3	
1-hexanol	13.0	0.80	613	0.12	1.3×10^3	
1-decanol	7.7	0.70	613	0.25	2.6×10^3	

[a] ε_s: static dielectric constant at 20 °C from ref 72. α: Kamlet–Taft parameter from ref 69. λ_f: fluorescence band maximum. Φ_f: fluorescence quantum yield. τ_f: fluorescence lifetime. τ_{TA}: excited-state lifetime determined from TA measurements. [b] Volume/volume ratio of the solvent mixture.

solvents and is comparable to the dielectric relaxation time of the solvent. As a consequence, most of the fluorescence takes place out of equilibrium, i.e., before the S_1 state has entirely relaxed, and thus the steady-state emission spectrum is at a higher energy than that from the fully relaxed excited state. The fluorescence quantum yields in protic solvents are generally smaller than in aprotic solvents with a similar $f(\varepsilon_s)$ value, the difference increasing with the polarity. This again is apparently connected with the H-bond donor properties of the solvent. Indeed, parameter α increases considerably when going from DeOH to water and, in the latter, only an upper limit of $\Phi_f = 3 \times 10^{-4}$ could be estimated.

In comparison, the fluorescence quantum yield of DPP2 is around 0.75 in both ACN and H_2O and is mostly independent of the polarity and H-bond donor strength of the solvent.

Time-Resolved Spectroscopy. The fluorescence decays of DPP2 in both ACN and water, measured by TCSPC, could be well reproduced using an exponential function with lifetimes, τ_f, of 5.2 and 5.5 ns, respectively. In aprotic solvents, the fluorescence decays of DPP1 were slow enough to be determined by TCSPC as well. As expected from the fluorescence quantum yields, τ_f depends on the solvent polarity and decreases from ca. 4 ns in apolar and moderately polar solvents to 460 ps in ACN (Table 1). The radiative time constant, calculated as $\tau_{rad} = \Phi_f/\tau_f$, is around 11 ns in all solvents, except in CHX where it amounts to 7.2 ns. This small difference could reflect an increase in the charge-transfer character of the $S_1 \leftarrow S_0$ transition in polar solvents.[73] On the other hand, the relatively constant value of τ_{rad} indicates that the solvent dependence of both Φ_f and τ_f arises mostly from nonradiative processes that are faster in polar solvents, as illustrated in Figure S3 which shows the nonradiative decay time, τ_{nr}, calculated as $\tau_{nr}^{-1} = \tau_f^{-1} - \tau_{rad}^{-1}$, as a function of $f(\varepsilon_s)$.

A much larger solvent dependence of the fluorescence lifetime is observed in alcohols, with the solubility of DPP1 in water being too small for a trustworthy measurement. In the longer alcohols, the fluorescence decay was slow enough to be reliably determined by TCSPC. In all cases, the decays were exponential with a lifetime decreasing from 2.6 ns in DeOH to 220 ps in EtOH (Table 1). The fluorescence dynamics in MeOH was investigated by FU. Measurements were performed every 20 nm between 560 to 700 nm, and the time profiles were analyzed globally (Figure 3A). The sum of two exponential functions was required to reproduce these profiles properly. The amplitude associated with the shorter lifetime,

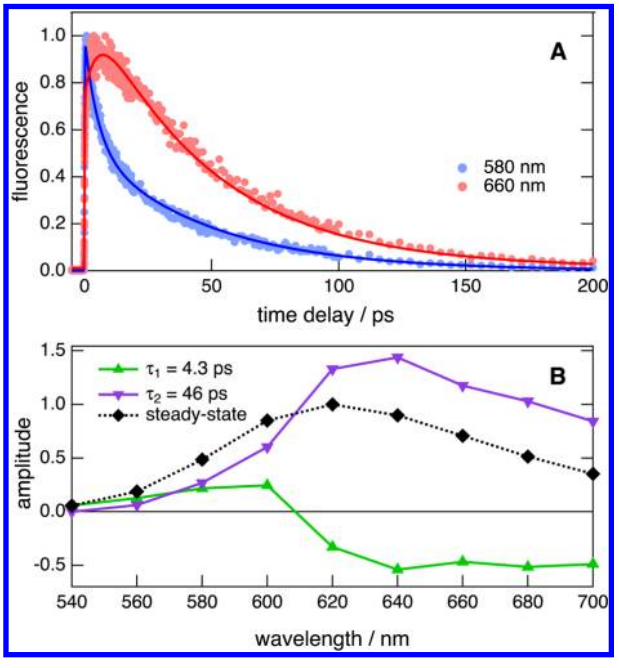

Figure 3. (A) Time profiles of the fluorescence intensity recorded at two wavelengths with DPP1 in MeOH and the best biexponental fits. (B) Decay-associated spectra obtained from a biexponential global analysis of the fluorescence time profiles; the steady-state spectrum is shown for comparison.

dx.doi.org/10.1021/jp506062j | J. Phys. Chem. B 2014, 118, 9952–9963

4.3 ps, is positive on the blue side of the fluorescence band and is negative on the other side, pointing to a red shift of the emission band (Figure 3B). This effect can be ascribed to a dynamic Stokes shift originating from the relaxation of the solvent around the excited molecules, with the 4.3 ps time constant being in good agreement with the solvation times reported in the literature.[74,75] Given the relatively large excess excitation energy of around 0.8 eV, vibrational relaxation could also partially contribute to this fast component.[76]

On the other hand, the amplitude associated with the longer time constant, 46 ps, is positive throughout the spectrum and can thus be ascribed to the decay of the excited-state population (Figure 3B). Biexponential global analysis of the FU time profiles in ACN yielded 1.6 and 460 ps time constants with decay-associated spectra very similar to those in MeOH, comforting the assignment of the shorter and longer time constants to solvent/vibrational relaxation and excited-state lifetime, respectively. As DPP1 is poorly soluble in water, FU measurements were performed in water/ACN (3:1) and water/MeOH (1:1) mixtures, and excited-state lifetimes of 15 and 13 ps were obtained, respectively. In view of these values and the fluorescence quantum yield (Table 1), the excited-state lifetime of DPP1 in water can be estimated to be smaller than 10 ps.

In all alcohols, the radiative time constant, τ_{rad}, is around 11 ns like in polar aprotic solvents, and thus the variation of the fluorescence lifetime arises from nonradiative processes. Compared to aprotic solvents of similar polarity, the nonradiative decay times, τ_{nr}, are substantially shorter in protic solvents and exhibit a much stronger dependence on polarity (Figure S3). This difference is again most probably connected to the H-bond donor strength of the solvents. The larger polarity dependence of τ_{nr} in protic solvents is due to the increase in both the α parameter and $f(\varepsilon_s)$ with decreasing alcohol length. Figure 4 confirms the good correlation between

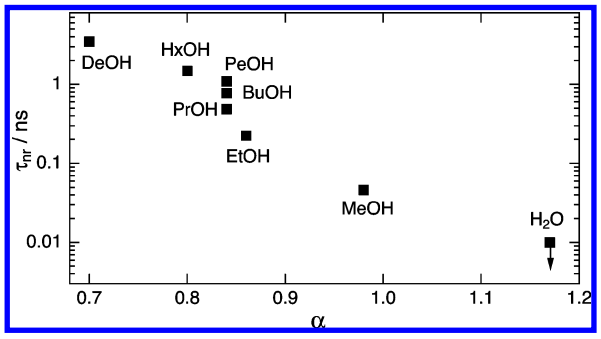

Figure 4. Correlation between the time constant of the nonradiative decay of the excited-state of DPP1 and parameter α reflecting the H-bond-donating ability of the solvent.

τ_{nr} and α. However, for the same α value, τ_{nr} is not constant but decreases with increasing solvent polarity. Therefore, both the polarity and the H-bond-donating ability of the solvent affect the excited-state dynamics of DPP1.

Figure 5 shows TA spectra recorded at several time delays after 400 nm excitation of DPP1 in ACN and a 1:1 water/ACN mixture, with those measured in MeOH and in EtOH being depicted in Figures S4 and S5. All spectra are dominated by a positive band peaking at around 720 nm and two negative bands centered at about 600 and 510 nm. Apart from shifts toward shorter and longer wavelengths of, respectively, the 720 and the 510 nm bands during the first 5 ps, no very significant

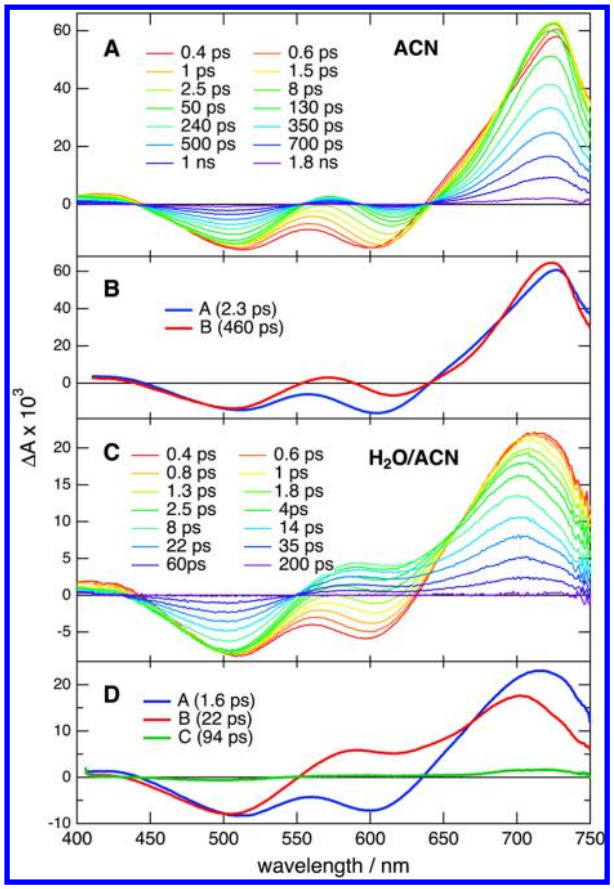

Figure 5. Transient absorption spectra recorded at various time delays after 400 nm excitation of DPP1 in (A) ACN, (C) a 1:1 water/ACN mixture, and (B, D) species-associated difference spectra obtained upon global target analysis assuming (B) an A → B → C or (D) an A → B → C → D scheme.

change in spectral shape can be observed, and all transient features decay to zero within 1 ns and 100 ps in ACN and water/ACN. From a comparison with the steady-state absorption and emission spectra, the high-energy negative band can be assigned to the bleach of the $S_1 \leftarrow S_0$ transition due to the depletion of the ground-state population, whereas the low-energy negative band can be ascribed to the $S_1 \rightarrow S_0$ stimulated emission. The initial red shift of the latter band arises from a dynamic Stokes shift caused by solvent relaxation. This process, together with vibrational relaxation, is probably responsible as well for the small spectral dynamics of the 720 nm band, which can be assigned to $S_n \leftarrow S_1$ absorption. In the water/ACN mixture, this band additionally exhibits a small red shift in the 8−30 ps time window. This effect most probably arises from the inhomogeneity of the solvent composition around DPP1. Those DPP1 molecules without water in their vicinity are longer lived than those surrounded by water, and their $S_n \leftarrow S_1$ absorption band is more red-shifted, as illustrated in Figure 5A.

Global target analysis was performed on these TA data assuming a series of consecutive exponential steps. In ACN, a simple A → B → C scheme, with C being the ground state, was enough to reproduce the TA spectra with 2.3 and 460 ps time constants for the A → B and B → C steps, respectively, with the species-associated difference spectra (SADS) shown in Figure 5B. The main differences between the A and B SADS are the position and intensity of the stimulated emission band and

dx.doi.org/10.1021/jp506062j | J. Phys. Chem. B 2014, 118, 9952−9963

the shape of the $S_n \leftarrow S_1$ absorption band. From the magnitude of the time constants and the shape of the SADS, species A and B can be interpreted as the unrelaxed and relaxed S_1 states, respectively. Although 400 nm excitation should coincide with a transition to an upper excited state, internal conversion is too fast for the initially populated state to be observed. The A → B → C scheme could not account for the slower red shift in the TA spectra in the water/ACN mixture. On the other hand, an A → B → C → D scheme, with D being the ground state, could successfully reproduce the data with 1.6, 22, and ∼90 ps time constants and the SADS shown in Figure 5D. Such a scheme is, in principle, not adequate to account for the inhomogeneity of the solvent composition around DPP1 discussed above, and a model with a distribution of parallel decay pathways, reflecting the distribution of environments around the molecule, should be applied. This is, however, not practically feasible, as this would require too many adjustable parameters. As a consequence, the SADS shown in Figure 5D should not be considered too literally. The first one should correspond to the unrelaxed S_1 state, whereas the second and third SADS should mostly reflect the relaxed S_1 state of DPP1 in water-rich and water-poor environments, respectively, with corresponding decay times of 22 and ca. 90 ps.

An A → B → C → D scheme was also required in MeOH and EtOH (Figures S4 and S5). In those cases, however, a third step had to be added to account for the multiphasic nature of the dielectric relaxation of alcohols.[74,77] As a consequence, species A is interpreted as the unrelaxed S_1 state, whereas species B and C correspond to partially and fully relaxed S_1 states, with the decay of the latter being listed in Table 1.

The following observations can be made from the TA measurements: (1) Although the excited-state lifetime of DPP1 in the water/ACN mixture and in short alcohols is much smaller than in ACN, no transient species other than the S_1 and the ground states could be identified. This indicates that, if the short excited-state lifetime in protic solvents is associated with an intermolecular quenching process, such as a proton transfer, then the decay of the product state to the ground state of DPP1 is much faster than the quenching itself. (2) The shape and position of the $S_n \leftarrow S_1$ absorption band depend noticeably on the solvent, especially when considering the SADS. In ACN, this band is the narrowest, with peaks initially at 727 nm shifting to 724 nm, i.e., by 50 cm^{-1}, upon relaxation. These effects are much more marked in protic solvents (EtOH, MeOH, and H_2O/ACN mixture) and increase with when going from EtOH to the H_2O/ACN mixture: the band is substantially broader than in ACN, its initial maximum is at shorter wavelengths, and the blue shift upon relaxation is on the order of 250 cm^{-1}.

The effect of deuteration of the protic solvents on the S_1 state dynamics of DPP1 was also investigated by performing TA measurements in MeOD and a 1:1 D_2O/ACN mixture. The TA spectra were very similar to those measured in the corresponding nondeuterated solvents and were analyzed in the same way. In MeOD, the lifetime of the relaxed S_1 state is longer than in MeOH and amounts to 54 vs 45 ps in MeOH (Table 1). A similar difference was observed in D_2O/ACN, with a excited-state lifetime of 26 ps vs 22 ps in H_2O/ACN. This corresponds to a kinetic isotope effect of about 1.2.

These bulk measurements demonstrate the spectacular change in the excited-state dynamics of these DPP dyes upon introducing push−pull substituents. Although the excited state of DPP1 possesses charge-transfer character, the dependence of its dynamics on the dielectric constant of the environment is not sufficient to make it a really useful polarity probe. However, the strong dependence of its S_1 lifetime on the α parameter of the solvent makes this molecule a powerful H-bonding probe.

The mechanism responsible for this dependence on the H-bond donor properties of the solvent is not fully understood, although this effect is already documented.[50,78−85] Molecules undergoing H-bond-assisted nonradiative relaxation are characterized by the presence of H-bond accepting groups, such as carbonyl and nitro groups, and a substantial charge-transfer character of the first excited state. All of these ingredients are present in DPP1 but not in DPP2, which lacks the charge-transfer excited state and is thus not sensitive to H-bond interactions. According to the quantum chemical calculations, the electronic density on one of the carbonyl oxygen atoms decreases whereas that on the other increases upon $S_1 \leftarrow S_0$ excitation of DPP1. On the other hand, the electronic density on both oxygen atoms of DPP2 decreases upon excitation.

According to the density distribution obtained for DPP1, one should expect a prompt strengthening of one of the H-bonds of this molecule with the solvent upon excitation, which results in an increased coupling of the excited molecule to the H-bonding network formed by the solvent. This enhanced coupling increases the number of vibrational degrees of freedom that can act as energy-accepting modes. Such a mechanism could explain the decrease in the nonradiative decay time with both the polarity and H-bond donor strength of the solvent. Indeed, the excited-state lifetime of DPP1 is shortened considerably by going from PeOH to BuOH and PrOH, although the α parameter of these three solvents remains constant. A limit of this mechanism would be an intermolecular proton transfer followed by an ultrafast back-transfer to the ground state. Although this could be envisaged in water, there is presently no experimental evidence in favor of or against such a process. The observed kinetic isotope effect is an unambiguous indication that the protic nature of the solvent plays a key role, but it does not allow a definite conclusion on the mechanism to be drawn. A kinetic isotope effect of similar size has also been observed with other molecules undergoing H-bond-assisted nonradiative decay.[50,78,83] On the other hand, kinetic isotope effects ranging from essentially 1 up to about 4 have been reported for intermolecular excited-state proton-transfer reactions.[86−89]

DPP1 at the Dodecane/(Heavy) Water Interface. The stationary SSHG spectrum recorded with DPP1 at the dodecane/water interface is depicted in Figure 6A together with the electronic absorption spectra in water and CHX. The SSHG and the $S_1 \leftarrow S_0$ absorption bands have a similar shape, but the former peaks at shorter wavelength, i.e., around 470 nm vs 498 and 512 nm, respectively. This difference cannot simply be interpreted in terms of the specific environment of DPP1 at the interface as these bands originate from intrinsically different processes. The SSHG intensity arises from a two-photon $S_1 \leftarrow S_0$ resonance, and its band maximum could coincide with a vibronic transition. Such a difference in the Franck−Condon envelope for one- and two-photon absorption has already been reported.[90]

Figure 6B shows polarization profiles obtained by measuring the intensity of the SSHG signal components parallel (p) or perpendicular (s) to the plane of incidence while continuously varying the polarization of the probe field. The shape of these profiles depends on the relative magnitude of the three nonvanishing tensor elements of $\vec{\vec{\chi}}^{(2)}$.[91] These measurements were carried out to determine the best set of polarizations for

dx.doi.org/10.1021/jp506062j | J. Phys. Chem. B 2014, 118, 9952−9963

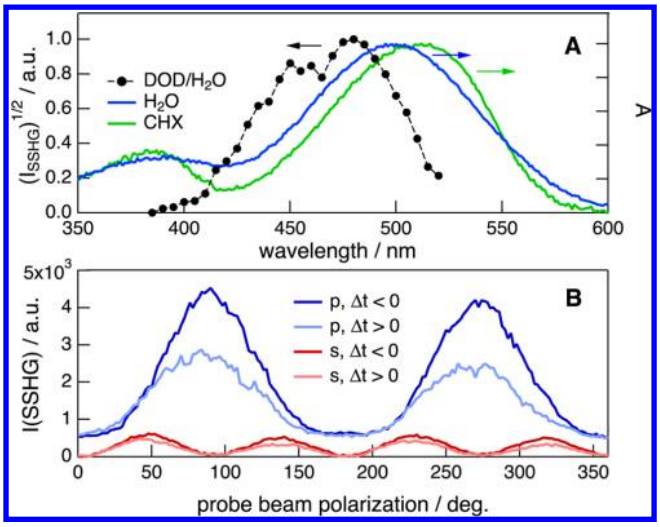

Figure 6. (A) Stationary SSHG spectrum measured with DPP1 at the dodecane/water interface and electronic absorption spectra of DPP1 in water and cyclohexane. (B) Dependence of the parallel (p) and perpendicular (s) components of the SSHG signal on the probe beam polarization measured with DPP1 at the dodecane/water interface at positive (10 ps) and negative (−20 ps) time delays between the pump and probe pulses.

the TR-SSHG measurements. As illustrated in Figure 6B, the strongest SSHG intensity change upon 510 nm excitation of DPP1 occurs when measuring the p component of the signal and probing with s polarization (90°). The resulting signal is then proportional to $|\chi^{(2)}_{zxx}|^2$. Photoinduced changes could also be measured with the s component of the signal upon probing with light polarized at 45°, i.e., upon probing $|\chi^{(2)}_{xzx}|^2$. However, since the overall signal intensity was much smaller, this polarization configuration was not further applied.

The SSHG signal measured with DPP2 at the dodecane/water interface was too small to obtain reliable data. This weak second-order nonlinear response agrees with the centrosymmetric nature of this molecule. This is also confirmed by quantum chemistry calculations of the second-order hyperpolarizability tensor, $\vec{\beta}$ (Table S1). For DPP1, the main tensor element is $\beta_{XXX} = 2.4 \times 10^4$ atomic units, where X is the long molecular axis (Figure S6). The other tensor elements are below 550 atomic units, whereas for DPP2 all of them are smaller (Table S1).

Figure 7 shows a TR-SSHG signal profile, $S(t)$, measured at 400 nm, i.e., upon 800 nm probing, after 510 nm excitation of

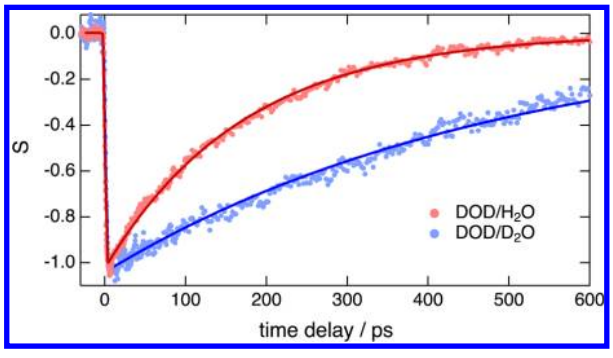

Figure 7. TR-SSHG profiles, $S(t)$, measured at 400 nm at the dodecane/water and dodecane/heavy-water interfaces upon 510 nm excitation of DPP1 and the best exponential fits.

DPP1 at the dodecane/water interface, with a time profile of the unprocessed SSHG intensity being depicted in Figure S7. Probing at 900 and 950 nm yielded identical profiles within the limit of error (Figure S8). As photoexcitation results in a decrease in the SSHG intensity, the observed time dependence should mostly reflect the ground-state recovery dynamics of DPP1. A comparison with the TA spectra suggests that a contribution to the TR-SSHG signal from an $S_n \leftarrow S_1$ resonance cannot be excluded. However, as no other transient than the S_1 state could be identified in the TA spectra, such a contribution from the excited state should have no significant influence on the dynamics, as it is mostly associated with the decay of the excited state to the ground state. These time profiles could be satisfactorily reproduced with the convolution of a Gaussian function, accounting for the instrument response, with an exponential decay. From measurements performed with different samples and at different days, a ground-state recovery time of 175 ± 25 ps is obtained. This value is considerably larger than the upper-limit value of 10 ps estimated in bulk water. Nevertheless, it is still much smaller than the excited-state decay times in aprotic solvents, indicating that the chromophoric part of DPP1 at the interface is not entirely immersed in the hydrophobic phase.

The above conclusion for the location of DPP1 is comforted by MD simulations, which reveal that this molecule partitions at the interface with the poly(ethylene glycol) chains immersed in the aqueous phase and the DPP unit in contact with both phases (Figure 8). The affinity of this molecule for the interface

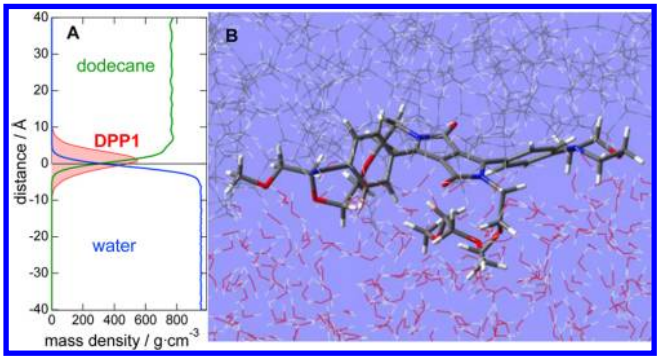

Figure 8. (A) Density profiles of dodecane, water, and the chromophoric center of DPP1 scaled by a factor 6. (B) MD simulations of the passive distribution of DPP1 between bulk dodecane and water.

is also confirmed by additional MD simulations, which show that, after having been placed in bulk water or bulk dodecane, it moves to the surface. Furthermore, an analysis of MD trajectories obtained in aqueous solution and at the dodecane/water interface indicates that the probability for DPP1 to be H-bonded drops from 65% in water to 19% at the interface. The same procedure but for the S_1 state reveals that the probability of H-bond formation increases to 73% in bulk water and 27% at the interface.

Decisive evidence of the ability of DPP1 to form H-bonds at the interface comes from TR-SSHG measurements performed at the dodecane/heavy-water interface, which reveal an important slowing down of the ground-state recovery dynamics compared to the dodecane/water interface, with a time constant of 475 ± 30 ps (Figure 7). This corresponds to a kinetic isotope effect of 2.7, which is more than twice as large as that measured in the D_2O/ACN mixture and MeOD. It

dx.doi.org/10.1021/jp506062j | J. Phys. Chem. B 2014, 118, 9952−9963

unambiguously points to the involvement of H bonds in the excited-state decay of the molecule at the interface.

The increase in the S_1 state lifetime by a factor of nearly 20 found by going from bulk water to the dodecane/water interface cannot be entirely accounted for by the limited access of DPP1 to water, as the H-bonding probability should, according to the MD simulations, decrease by a factor of ca. 3 only. Moreover, a limited exposure to water cannot explain the larger kinetic isotope effect measured at the interface. Several reasons can be proposed to explain this difference: (1) A strengthened H-bond network of interfacial water: although DPP1 is in contact with the aqueous phase, H-bond interactions with interfacial water are less efficient than with bulk water because the bonds between interfacial water molecules are stronger and thus favored relative to those between water and DPP1. Whereas the H-bond strength at the air/water interface is still debated,[28,92−94] there is a general consensus that the H-bond network of water at hydrophobic surfaces is significantly enhanced.[1,9,95,96] (2) Differences in vibrational frequencies of interfacial and bulk water: the interfacial vibrational spectrum in the O−H stretching region has been shown to differ from that of bulk water.[1,9,95,96] Consequently, interfacial water might be a less efficient energy-accepting bath than bulk water. (3) A lower local polarity: the above-described bulk measurements indicate that both the polarity and the H-bond donor strength of the solvent affect the efficiency of the nonradiative decay of the DPP1 excited state. SSHG measurements using solvatochromic probes suggest that the local electric field experienced by a molecule adsorbed at a water/alkane or air/water interface is substantially lower than that in bulk water.[97−99] A lower local polarity could decrease the charge-transfer character of the S_1 state of DPP1 and thus weaken its H-bond acceptor ability.

The first two effects should contribute to the substantial slowing down of the dynamics upon deuteration. Deuterium bonds are known to be stronger than hydrogen bonds, and thus the competition between interfacial water−water and water−DPP1 bonds should be further in disfavor of the latter in D_2O.[100,101] Of course, isotopic substitution has a major impact on the vibrational modes of water and on their coupling with those of DPP1.

Our results agree well with those reported for eosin B at the dodecane/water and decanol/water interfaces.[102] At both interfaces, a strong slowing down of the excited-state lifetime relative to that of bulk water, where H-bond-assisted nonradiative decay is operative,[84] was observed. In the case of eosin B, however, deuterium substitution was not investigated and MD simulations were not performed, and thus the accessibility of water molecules to the H-bond sites of eosin B could not be evidenced.

On the other hand, our hypothesis of competition for H bonding is in apparent contradiction to the conclusions of an investigation where the blue shift of the SSHG spectrum of *N*-methyl-*p*-methoxyaniline at the water/CCl_4 interface relative to the electronic absorption spectrum in bulk water was interpreted as a stronger H-bond interaction with interfacial water.[103] However, both results can be reconciled by keeping in mind that the effect should strongly depend on the nature of the probe, e.g., its H-bond-accepting ability and its exact location at the interface. The interfacial SSHG spectrum of DPP1 measured here is also blue-shifted relative to its absorption spectrum in water, but as mentioned above, this effect is attributed to the difference in one- and two-photon absorption spectra that are often observed.

CONCLUDING REMARKS

This investigation illustrates how the addition of relatively weak push−pull substituents to a chromophore with H-bonding sites can totally change its excited-state properties. In the case of the DPP derivative investigated here, the charge-transfer character of the $S_1 \leftarrow S_0$ transition results in an increase in the electronic density on one of the H-bonding sites and thus reinforces the coupling of the molecule with the H-bond network of protic solvents, favoring the nonradiative relaxation of the excited state. The results presented here reveal that both the solvent polarity and the H-bond donor strength enhance this effect, which is thus the strongest in water. Although the number of cases where H-bond-assisted nonradiative deactivation is being observed is increasing, its exact mechanism still needs to be elucidated. Time-resolved vibrational spectroscopy is currently being applied in our laboratory to try to answer this question.

The sensitivity of this push−pull DPP derivative to the environment makes it an ideal SSHG probe for investigating H-bond interactions with interfacial water. Going from bulk water to the dodecane/water interface results in a slowing down of the excited-state dynamics by a factor of ca. 20. Moreover, going to the dodecane/heavy-water interface leads to a further slowing down by a factor of about 3. The latter observation as well as the MD simulations indicate that the H-bonding sites of the molecule at the interface do interact with water. Therefore, we explain the relative inefficiency of the H-bond-assisted nonradiative deactivation at the interface not by a strongly reduced exposure of the probe to the aqueous phase but rather by the strengthening of the interfacial water−water H-bond network that is detrimental to the bonds with the DPP probe. Other factors, such as a lower local polarity experienced by the probe, could also contribute. Further investigations with probes characterized by different H-bond acceptor strengths or a different location at the interfaces as well as with "pure" polarity probes are needed before a comprehensive picture of the intrinsic properties of the water/liquid interface can be obtained. The present investigation is an illustration of how photochemical reactivity can change by going from the bulk phase to an interface.

ASSOCIATED CONTENT

Supporting Information

Details on the synthesis of DPP1 and DPP2; absorption and emission spectra of DPP1 in several solvents and a solvatochromic plot; solvent polarity dependence of the nonradiative decay time; transient absorption spectra of DPP1 in MeOH and EtOH and species-associated spectra; second-order hyperpolarizability tensor elements; and raw SSHG data. This material is available free of charge via the Internet at http://pubs.acs.org.

AUTHOR INFORMATION

Corresponding Author

*E-mail: eric.vauthey@unige.ch.

Notes

The authors declare no competing financial interest.

■ ACKNOWLEDGMENTS

This work was supported by the Swiss National Science Foundation through project no. 200020-147098 and the University of Geneva.

■ REFERENCES

(1) Gragson, D. E.; Richmond, G. L. Investigations of the Structure and Hydrogen Bonding of Water Molecules at Liquid Surfaces by Vibrational Sum Frequency Spectroscopy. *J. Phys. Chem. B* **1998**, *102*, 3847−3861.
(2) Mitrinovic, D. M.; Zhang, Z.; Williams, S. M.; Huang, Z.; Schlossman, M. L. X-Ray Reflectivity Study of the Water-Hexane Interface. *J. Phys. Chem. B* **1999**, *103*, 1779−1782.
(3) Pal, S. K.; Zewail, A. H. Dynamics of Water in Biological Recognition. *Chem. Rev.* **2004**, *104*, 2099−2123.
(4) McGuire, J.; Shen, Y. R. Ultrafast Vibrational Dynamics at Water Interfaces. *Science* **2006**, *313*, 1945−1948.
(5) Ball, P. Water as an Active Constituent in Cell Biology. *Chem. Rev.* **2007**, *108*, 74−108.
(6) Moore, F. G.; Richmond, G. L. Integration or Segregation: How Do Molecules Behave at Oil/Water Interfaces? *Acc. Chem. Res.* **2008**, *41*, 739−748.
(7) Persson, E.; Halle, B. Cell Water Dynamics on Multiple Time Scales. *Proc. Natl. Acad. Sci. U.S.A.* **2008**, *105*, 6266−6271.
(8) McFearin, C. L.; Beaman, D. K.; Moore, F. G.; Richmond, G. L. From Franklin to Today: Toward a Molecular Level Understanding of Bonding and Adsorption at the Oil−Water Interface. *J. Phys. Chem. C* **2009**, *113*, 1171−1188.
(9) Sovago, M.; Kramer Campen, R.; Bakker, H. J.; Bonn, M. Hydrogen Bonding Strength of Interfacial Water Determined with Surface Sum-Frequency Generation. *Chem. Phys. Lett.* **2009**, *470*, 7−12.
(10) Campen, R. K.; Ngo, T. T. M.; Sovago, M.; Ruysschaert, J.-M.; Bonn, M. Molecular Restructuring of Water and Lipids upon the Interaction of DNA with Lipid Monolayers. *J. Am. Chem. Soc.* **2010**, *132*, 8037−8047.
(11) Eftekhari-Bafrooei, A.; Borguet, E. Effect of Hydrogen-Bond Strength on the Vibrational Relaxation of Interfacial Water. *J. Am. Chem. Soc.* **2010**, *132*, 3756−3761.
(12) Mancinelli, R.; Bruni, F.; Ricci, M. A.; Imberti, S. Microscopic Structure of Water in a Water/Oil Emulsion. *J. Chem. Phys.* **2013**, *138*, 204503.
(13) Nihonyanagi, S.; Mondal, J. A.; Yamaguchi, S.; Tahara, T. Structure and Dynamics of Interfacial Water Studied by Heterodyne-Detected Vibrational Sum-Frequency Generation. *Annu. Rev. Phys. Chem.* **2014**, *64*, 579−603.
(14) Breslow, R. Hydrophobic Effects on Simple Organic Reactions in Water. *Acc. Chem. Res.* **1991**, *24*, 159−164.
(15) Li, C. J. Organic Reactions in Aqueous Media - With a Focus on Carbon-Carbon Bond Formation. *Chem. Rev.* **1993**, *93*, 2023−2035.
(16) Gajewski, J. J. The Claisen Rearrangement. Response to Solvents and Substituents: The Case for Both Hydrophobic and Hydrogen Bond Acceleration in Water and for a Variable Transition State. *Acc. Chem. Res.* **1997**, *30*, 219−225.
(17) Narayan, S.; Muldoon, J.; Finn, M. G.; Fokin, V. V.; Kolb, H. C.; Sharpless, K. B. On Water": Unique Reactivity of Organic Compounds in Aqueous Suspension. *Angew. Chem., Int. Ed.* **2005**, *44*, 3275−3279.
(18) Shapiro, N.; Vigalok, A. Highly Efficient Organic Reactions "on Water", "in Water", and Both. *Angew. Chem., Int. Ed.* **2008**, *47*, 2849−2852.
(19) Jung, Y.; Marcus, R. A. On the Theory of Organic Catalysis "on Water. *J. Am. Chem. Soc.* **2007**, *129*, 5492−5502.
(20) Zheng, Y.; Zhang, J. Catalysis in the Oil Droplet/Water Interface for Aromatic Claisen Rearrangement. *J. Phys. Chem. A* **2010**, *114*, 4325−4333.
(21) Thomas, L. L.; Tirado-Rives, J.; Jorgensen, W. L. Quantum Mechanical/Molecular Mechanical Modeling Finds Diels−Alder Reactions Are Accelerated Less on the Surface of Water Than in Water. *J. Am. Chem. Soc.* **2010**, *132*, 3097−3104.
(22) Wang, Y.; Hodas, N. O.; Jung, Y.; Marcus, R. A. Microscopic Structure and Dynamics of Air/Water Interface by Computer Simulations-Comparison with Sum-Frequency Generation Experiments. *Phys. Chem. Chem. Phys.* **2011**, *13*, 5388−5393.
(23) Du, Q.; Superfine, R.; Seysz, E.; Shen, Y. R. Vibrational Spectroscopy of Water at the Vapor/Water Interface. *Phys. Rev. Lett.* **1993**, *70*, 2313−2316.
(24) Scatena, L. F.; Brown, M. G.; Richmond, G. L. Water at Hydrophobic Surfaces: Weak Hydrogen Bonding and Strong Orientation Effects. *Science* **2001**, *292*, 908−912.
(25) Fan, Y.; Chen, X.; Yang, L.; Cremer, P. S.; Gao, Y. Q. On the Structure of Water at the Aqueous/Air Interface. *J. Phys. Chem. B* **2009**, *113*, 11672−11679.
(26) Chen, X.; Hua, W.; Huang, Z.; Allen, H. C. Interfacial Water Structure Associated with Phospholipid Membranes Studied by Phase-Sensitive Vibrational Sum Frequency Generation Spectroscopy. *J. Am. Chem. Soc.* **2010**, *132*, 11336−11342.
(27) Zhang, Z.; Piatkowski, L.; Bakker, H. J.; Bonn, M. Ultrafast Vibrational Energy Transfer at the Water/Air Interface Revealed by Two-Dimensional Surface Vibrational Spectroscopy. *Nat. Chem.* **2011**, *3*, 888−893.
(28) Stiopkin, I. V.; Weeraman, C.; Pieniazek, P. A.; Shalhout, F. Y.; Skinner, J. L.; Benderskii, A. V. Hydrogen Bonding at the Water Surface Revealed by Isotopic Dilution Spectroscopy. *Nature* **2011**, *474*, 192−195.
(29) Eisenthal, K. B. Equilibrium and Dynamic Processes at Interfaces by Second Harmonic and Sum Frequency Generation. *Annu. Rev. Phys. Chem.* **1992**, *43*, 627−61.
(30) Nagatani, H.; Piron, A.; Brevet, P.-F.; Fermin, D. J.; Girault, H. H. Surface Second Harmonic Generation of Cationic Water-Soluble Porphyrins at the Polarized Water|1,2-Dichloroethane Interface. *Langmuir* **2002**, *18*, 6647−6652.
(31) Steel, W. H.; Walker, R. A. Measuring Dipolar Width across Liquid-Liquid Interfaces with 'Molecular Rulers'. *Nature* **2003**, *424*, 296−299.
(32) Sekiguchi, K.; Yamaguchi, S.; Tahara, T. Femtosecond Time-Resolved Electronic Sum-Frequency Generation Spectroscopy: A New Method to Investigate Ultrafast Dynamics at Liquid Interfaces. *J. Chem. Phys.* **2008**, *128*, 114715.
(33) Yamaguchi, S.; Tahara, T. Heterodyne-Detected Electronic Sum Frequency Generation: "Up" versus "Down" Alignment of Interfacial Molecules. *J. Chem. Phys.* **2008**, *129*, 101102.
(34) Richert, S.; Fedoseeva, M.; Vauthey, E. Ultrafast Photoinduced Dynamics at Air/Liquid and Liquid/Liquid Interfaces. *J. Phys. Chem. Lett.* **2012**, *3*, 1635−1642.
(35) Steinhurst, D. A.; Baronavski, A. P.; Owrutsky, J. C. Transient Second Harmonic Generation from Oxazine Dyes at the Air/Water Interface. *J. Phys. Chem. B* **2002**, *106*, 3160−3165.
(36) Fedoseeva, M.; Richert, S.; Vauthey, E. Excited-State Dynamics of Organic Dyes at Liquid-Liquid Interfaces. *Langmuir* **2012**, *28*, 11291−11301.
(37) Fedoseeva, M.; Fita, P.; Vauthey, E. Excited-State Dynamics of Charged Dyes at Alkane/Water Interfaces in the Presence of Salts and Ionic Surfactants. *Langmuir* **2013**, *29*, 14865−14872.
(38) Martin-Gassin, G.; Villamaina, D.; Vauthey, E. Nonradiative Deactivation of Excited Hemicyanines Studied with Submolecular Spatial Resolution by Time-Resolved Surface Second Harmonic Generation at Liquid-Liquid Interfaces. *J. Am. Chem. Soc.* **2011**, *133*, 2358−2361.
(39) Shi, X.; Borguet, E.; Tarnovsky, A. N.; Eisenthal, K. B. Ultrafast Dynamics and Structure at Aqueous Interfaces by Second Harmonic Generation. *Chem. Phys.* **1996**, *205*, 167−178.
(40) Fita, P.; Punzi, A.; Vauthey, E. Local Viscosity of Binary Water +Glycerol Mixtures at Liquid/Liquid Interfaces Probed by Time-Resolved Surface Second Harmonic Generation. *J. Phys. Chem. C* **2009**, *113*, 20705−20712.

(41) Sen, P.; Yamaguchi, S.; Tahara, T. Ultrafast Dynamics of Malachite Green at the Air-Water Interface Studied by Femtosecond Time-Resolved Electronic Sum Frequency Generation (TR-ESFG): an Indicator for Local Viscosity. *Faraday Discuss.* **2010**, *145*, 411−428.
(42) Hao, Z.; Iqbal, A. Some Aspects of Organic Pigments. *Chem. Soc. Rev.* **1997**, *26*, 203−213.
(43) Bijleveld, J. C.; Zoombelt, A. P.; Mathijssen, S. G. J.; Wienk, M. M.; Turbiez, M.; de Leeuw, D. M.; Janssen, R. A. J. Poly-(diketopyrrolopyrrole−terthiophene) for Ambipolar Logic and Photovoltaics. *J. Am. Chem. Soc.* **2009**, *131*, 16616−16617.
(44) Woo, C. H.; Beaujuge, P. M.; Holcombe, T. W.; Lee, O. P.; Fréchet, J. M. J. Incorporation of Furan into Low Band-Gap Polymers for Efficient Solar Cells. *J. Am. Chem. Soc.* **2010**, *132*, 15547−15549.
(45) Qu, S.; Tian, H. Diketopyrrolopyrrole (DPP)-Based Materials for Organic Photovoltaics. *Chem. Commun.* **2012**, *48*, 3039−3051.
(46) Banerji, N.; Wang, M.; Fan, J.; Chesnut, E. S.; Wudl, F.; Moser, J.-E. Sensitization of Fullerenes by Covalent Attachment of a Diketopyrrolopyrrole Chromophore. *J. Mater. Chem.* **2012**, *22*, 13286−13294.
(47) Nowak-Krol, A.; Grzybowski, M.; Romiszewski, J.; Drobizhev, M.; Wicks, G.; Chotkowski, M.; Rebane, A.; Gorecka, E.; Gryko, D. T. Strong Two-Photon Absorption Enhancement in a Unique Bis-Porphyrin Bearing a Diketopyrrolopyrrole Unit. *Chem. Commun.* **2013**, *49*, 8368−8370.
(48) Brouwer, A. M. Standards for Photoluminescence Quantum Yield Measurements in Solution. *Pure Appl. Chem.* **2011**, *83*, 2213−2228.
(49) Muller, P.-A.; Högemann, C.; Allonas, X.; Jacques, P.; Vauthey, E. Deuterium Isotope Effect on the Charge Recombination Dynamics of Contact Ion Pairs Formed by Electron Transfer Quenching in Acetonitrile. *Chem. Phys. Lett.* **2000**, *326*, 321−327.
(50) Fürstenberg, A.; Vauthey, E. Excited State Dynamics of the Fluorescent Probe Lucifer Yellow in Liquid Solutions in in Heterogeneous Media. *Photochem. Photobiol. Sci.* **2005**, *4*, 260−267.
(51) Morandeira, A.; Engeli, L.; Vauthey, E. Ultrafast Charge Recombination of Photogenerated Ion Pairs to an Electronic Excited State. *J. Phys. Chem. A* **2002**, *106*, 4833−4837.
(52) Duvanel, G.; Grilj, J.; Chaumeil, H.; Jacques, P.; Vauthey, E. Ultrafast Excited-State Dynamics of a Series of Zwitterionic Pyridinium Phenoxides with Increasing Sterical Hindering. *Photochem. Photobiol. Sci.* **2010**, *9*, 908−915.
(53) Lang, B.; Angulo, G.; Vauthey, E. Ultrafast Solvation Dynamics of Coumarin 153 in Imidazolium Based Ionic Liquids. *J. Phys. Chem. A* **2006**, *110*, 7028−7034.
(54) Duvanel, G.; Banerji, N.; Vauthey, E. Excited-State Dynamics of Donor-Acceptor Bridged Systems Containing a Boron-Dipyrromethene Chromophore: Interplay between Charge Separation and Reorientational Motion. *J. Phys. Chem. A* **2007**, *111*, 5361−5369.
(55) Banerji, N.; Duvanel, G.; Perez-Velasco, A.; Maity, S.; Sakai, N.; Matile, S.; Vauthey, E. Excited-State Dynamics of Hybrid Multichromophoric Systems: Toward an Excitation Wavelength Control of the Charge Separation Pathways. *J. Phys. Chem. A* **2009**, *113*, 8202−8212.
(56) Fedoseeva, M.; Letrun, R.; Vauthey, E. Excited-State Dynamics of Rhodamine 6G in Aqueous Solution and at the Dodecane/Water Interface. *J. Phys. Chem. B* **2014**, *18*, 5184−5193.
(57) Punzi, A.; Martin-Gassin, G.; Grilj, J.; Vauthey, E. Effect of Salt on the Excited-State Dynamics of Malachite Green in Bulk Aqueous Solutions and at Air/Water Interfaces: a Femtosecond Transient Absorption and Surface Second Harmonic Generation Study. *J. Phys. Chem. C* **2009**, *113*, 11822−11829.
(58) Zhao, Y.; Truhlar, D. The M06 Suite of Density Functionals for Main Group Thermochemistry, Thermochemical Kinetics, Noncovalent Interactions, Excited States, and Transition Elements: Two New Functionals and Systematic Testing of Four M06-Class Functionals and 12 other Functionals. *Theor. Chem. Acc.* **2008**, *120*, 215−241.
(59) Lee, C.; Yang, W.; Parr, R. G. Development of the Colle-Salvetti Correlation-Energy Formula into a Functional of the Electron Density. *Phys. Rev. B* **1988**, *37*, 785−789.
(60) Frisch, M. J.; Trucks, G. W.; Schlegel, H. B.; Scuseria, G. E.; Robb, M. A.; Cheeseman, J. R.; Scalmani, G.; Barone, V.; Mennucci, B.; Petersson, G. A., et al. *Gaussian 09*, revision C1; Gaussian, Inc.: Wallingford, CT, 2010.
(61) Siu, S. W. I.; Pluhackova, K.; Böckmann, R. A. Optimization of the OPLS-AA Force Field for Long Hydrocarbons. *J. Chem. Theory Comput.* **2012**, *8*, 1459−1470.
(62) Hermans, J.; Berendsen, H. J. C.; Van Gunsteren, W. F.; Postma, J. P. M. A Consistent Empirical Potential for Water−Protein Interactions. *Biopolymers* **1984**, *23*, 1513−1518.
(63) Berendsen, H. J. C.; Postma, J. P. M.; van Gunsteren, W. F.; DiNola, A.; Haak, J. R. Molecular Dynamics with Coupling to an External Bath. *J. Chem. Phys.* **1984**, *81*, 3684−3690.
(64) Darden, T.; York, D.; Pedersen, L. Particle Mesh Ewald: An N x log(N) Method for Ewald Sums in Large Systems. *J. Chem. Phys.* **1993**, *98*, 10089−10092.
(65) Hess, B.; Bekker, H.; Berendsen, H. J. C.; Fraaije, J. G. E. M. LINCS: A Linear Constraint Solver for Molecular Simulations. *J. Comput. Chem.* **1997**, *18*, 1463−1472.
(66) Van Der Spoel, D.; Lindahl, E.; Hess, B.; Groenhof, G.; Mark, A. E.; Berendsen, H. J. C. GROMACS: Fast, Flexible, and Free. *J. Comput. Chem.* **2005**, *26*, 1701−1718.
(67) Rochat, A. C.; Cassar, L.; Iqbal, A. *Preparation of Pyrrolo(3,4-c) pyrroles*. Eur. Pat. Appl. 94911, 1983.
(68) Taft, R. W.; Kamlet, M. J. The Solvatochromic Comparison Method. 2. The Alpha-Scale of Solvent Hydrogen-Bond donor (HBD) Acidities. *J. Am. Chem. Soc.* **1976**, *98*, 2886−94.
(69) Marcus, Y. The Properties of Organic Liquids that are Relevant to their Use as Solvating Solvents. *Chem. Soc. Rev.* **1993**, *22*, 409−416.
(70) Onsager, L. Electric Moments of Molecules in Liquids. *J. Am. Chem. Soc.* **1936**, *58*, 1486−1493.
(71) Suppan, P. Solvatochromic Shifts: the Influence of the Medium on the Energy of Electronic States. *J. Photochem. Photobiol.* **1990**, *A50*, 293−330.
(72) Wohlfahrt, C.; Madelung, O. *Static Dielectric Constants of Pure Liquids and Binary Liquid Mixtures*; Springer: Berlin, 1991.
(73) Banerji, N.; Angulo, G.; Barabanov, I. I.; Vauthey, E. Intramolecular Charge-Transfer Dynamics in Covalently Linked Perylene-Dimethylaniline and Cyanoperylene-Dimethylaniline. *J. Phys. Chem. A* **2008**, *112*, 9665−9674.
(74) Horng, M. L.; Gardecki, J. A.; Papazyan, A.; Maroncelli, M. Subpicosecond Measurements of Polar Solvation Dynamics: Coumarin 153 Revisited. *J. Phys. Chem.* **1995**, *99*, 17311−17337.
(75) Gumy, J. C.; Nicolet, O.; Vauthey, E. Investigation of the Solvation Dynamics of an Organic Dye in Polar Solvents Using the Femtosecond Transient Grating Technique. *J. Phys. Chem. A* **1999**, *103*, 10737−10743.
(76) Pigliucci, A.; Duvanel, G.; Daku, L. M. L.; Vauthey, E. Investigation of the Influence of Solute-solvent Interactions on the Vibrational Energy Relaxation Dynamics of Large Molecules in Liquids. *J. Phys. Chem. A* **2007**, *111*, 6135−6145.
(77) Rosspeintner, A.; Lang, B.; Vauthey, E. Ultrafast Photochemistry in Liquids. *Annu. Rev. Phys. Chem.* **2013**, *64*, 247−271.
(78) Flom, S. R.; Barbara, P. F. Proton Transfer and Hydrogen Bonding in the Internal Conversion of S1 Anthraquinones. *J. Phys. Chem.* **1985**, *89*, 4489−4494.
(79) Nishiya, T.; Yamauchi, S.; Hirota, N.; Baba, M.; Hanazaki, I. Fluorescence Study of the Intramolecularly Hydrogen-Bonded Molecules o-Hydroxyacetophenone and Salicylamide and Related Molecules. *J. Phys. Chem.* **1986**, *90*, 5730−5735.
(80) Yatsuhashi, T.; Inoue, H. Molecular Mechanism of Radiationless Deactivation of Aminoanthraquinones through Intermolecular Hydrogen Bonding Interaction with Alcohols and Hydroperoxydes. *J. Phys. Chem. A* **1997**, *101*, 8166−8173.
(81) Shimada, H.; Nakamura, A.; Yoshihara, T.; Tobita, S. Intramolecular and Intermolecular Hydrogen-Bonding Effects on

Photophysical Properties of 2′-Aminoacetophenone and its Derivatives in Solution. *Photochem. Photobiol. Sci.* **2005**, *4*, 367−375.
(82) Mohammed, O. F.; Vauthey, E. Excited-State Dynamics of Nitroperylene in Solution: Solvent and Excitation Wavelength Dependence. *J. Phys. Chem. A* **2008**, *112*, 3823−3830.
(83) Sherin, P. S.; Grilj, J.; Tsentalovitch, Y. P.; Vauthey, E. Ultrafast Excited-State Dynamics of Kynurenine, a UV Filter of the Human Eye. *J. Phys. Chem. B* **2009**, *113*, 4953−4962.
(84) Fita, P.; Fedoseeva, M.; Vauthey, E. Ultrafast Excited-State Dynamics of Eosin B: a Potential Probe of the Hydrogen-Bonding Properties of the Environment. *J. Phys. Chem. A* **2011**, *115*, 2465−2470.
(85) Lee, S. F.; Vérolet, Q.; Fürstenberg, A. Improved Super-Resolution Microscopy with Oxazine Fluorophores in Heavy Water. *Angew. Chem., Int. Ed.* **2013**, *52*, 8948−8951.
(86) Stryer, L. Excited-State Proton-Transfer Reactions. A Deuterium Isotope Effect on Fluorescence. *J. Am. Chem. Soc.* **1966**, *88*, 5708−5712.
(87) Chen, Q.; Walczak, W. J.; Barkley, M. D. Excited-State Proton Transfer from Solvent to Aromatic Carbons in Tomaymycin. *J. Am. Chem. Soc.* **1995**, *117*, 556−557.
(88) Pines, E., The Kinetic Isotope Effect in the Photodissociation Reaction of Excited-State Acids in Aqueous Solutions. In *Isotope Effects in Chemistry and Biology*; Kohen, A., Limbach, H.-H., Eds.; CRC Press: Boca Raton, FL, 2005; pp 451−464.
(89) Presiado, I.; Erez, Y.; Huppert, D. Excited-State Intermolecular Proton Transfer of the Firefly's Chromophore d-Luciferin. 2. Water−Methanol Mixtures. *J. Phys. Chem. A* **2010**, *114*, 9471−9479.
(90) Makarov, N. S.; Drobizhev, M.; Rebane, A. Two-Photon Absorption Standards in the 550−1600 nm Excitation Wavelength Range. *Opt. Express* **2008**, *16*, 4029−4047.
(91) Brevet, P. F. Phenomenological Three-Layer Model for Surface Second-Harmonic Generation at the Interface between Two Centrosymmetric Media. *J. Chem. Soc., Faraday Trans.* **1996**, *92*, 4547−4554.
(92) Raymond, E. A.; Tarbuck, T. L.; Brown, M. G.; Richmond, G. L. Hydrogen-Bonding Interactions at the Vapor/Water Interface Investigated by Vibrational Sum-Frequency Spectroscopy of HOD/H_2O/D_2O Mixtures and Molecular Dynamics Simulations. *J. Phys. Chem. B* **2002**, *107*, 546−556.
(93) Tian, C.-S.; Shen, Y. R. Isotopic Dilution Study of the Water/Vapor Interface by Phase-Sensitive Sum-Frequency Vibrational Spectroscopy. *J. Am. Chem. Soc.* **2009**, *131*, 2790−2791.
(94) Nihonyanagi, S.; Ishiyama, T.; Lee, T.-K.; Yamaguchi, S.; Bonn, M.; Morita, A.; Tahara, T. Unified Molecular View of the Air/Water Interface Based on Experimental and Theoretical $\chi^{(2)}$ Spectra of an Isotopically Diluted Water Surface. *J. Am. Chem. Soc.* **2011**, *133*, 16875−16880.
(95) Michael, D.; Benjamin, I. Molecular Dynamics Computer Simulations of Solvation Dynamics at Liquid/Liquid Interfaces. *J. Chem. Phys.* **2001**, *114*, 2817−2824.
(96) Strazdaite, S.; Versluis, J.; Backus, E. H. G.; Bakker, H. J. Enhanced Ordering of Water at Hydrophobic Surfaces. *J. Chem. Phys.* **2014**, *140*, 054711.
(97) Zimdars, D.; Eisenthal, K. B. Static and Dynamic Solvation at the Air/Water Interface. *J. Phys. Chem. B* **2001**, *105*, 3993−4002.
(98) Steel, W. H.; Damkaci, F.; Nolan, R.; Walker, R. A. Molecular Rulers: New Families of Molecules for Measuring Interfacial Widths. *J. Am. Chem. Soc.* **2002**, *124*, 4824−4831.
(99) Steel, W. H.; Walker, R. A. Solvent Polarity at an Aqueous/Alkane Interface: the Effect of Solute Identity. *J. Am. Chem. Soc.* **2003**, *125*, 1132.
(100) Scheiner, S.; Cuma, M. Relative Stability of Hydrogen and Deuterium Bonds. *J. Am. Chem. Soc.* **1996**, *118*, 1511−1521.
(101) Milhaud, J.; Bouchemal, N.; Rog, T.; Hantz, E. Deuteration of Water Enables Self-Organization of Phospholipid-Based Reverse Micelles. *ChemPhysChem* **2010**, *11*, 590−598.
(102) Fita, P.; Fedoseeva, M.; Vauthey, E. Hydrogen-Bond-Assisted Excited-State Deactivation at Liquid/Water Interfaces. *Langmuir* **2011**, *27*, 4645−4652.
(103) Siler, A. R.; Brindza, M. R.; Walker, R. A. Hydrogen-Bonding Molecular Ruler Surfactants as Probes of Specific Solvation at Liquid/Liquid Interfaces. *Anal. Bioanal. Chem.* **2009**, *395*, 1063−1073.